Xiaocen Kong,[1] Jing Yu,[1] Jianhua Bi,[1] Hanmei Qi,[1] Wenjuan Di,[1] Lin Wu,[1] Long Wang,[1] Juanmin Zha,[1] Shan Lv,[1] Feng Zhang,[2] Yan Li,[3] Fang Hu,[3] Feng Liu,[3] Hong Zhou,[4] Juan Liu,[1] and Guoxian Ding[1]

# Glucocorticoids Transcriptionally Regulate miR-27b Expression Promoting Body Fat Accumulation Via Suppressing the Browning of White Adipose Tissue

*Diabetes 2015;64:393–404 | DOI: 10.2337/db14-0395*

**Long-term glucocorticoid (GC) treatment induces central fat accumulation and metabolic dysfunction. We demonstrate that microRNA-27b (miR-27b) plays a central role in the pathogenesis of GC-induced central fat accumulation. Overexpression of miR-27b had the same effects as dexamethasone (DEX) treatment on the inhibition of brown adipose differentiation and the energy expenditure of primary adipocytes. Conversely, antagonizing miR-27b function prevented DEX suppression of the expression of brown adipose tissue–specific genes. GCs transcriptionally regulate miR-27b expression through a GC receptor–mediated direct DNA-binding mechanism, and miR-27b suppresses browning of white adipose tissue (WAT) by targeting the three prime untranslated region of Prdm16. In vivo, antagonizing miR-27b function in DEX-treated mice resulted in the efficient induction of brown adipocytes within WAT and improved GC-induced central fat accumulation. Collectively, these results indicate that miR-27b functions as a central target of GC and as an upstream regulator of Prdm16 to control browning of WAT and, consequently, may represent a potential target in preventing obesity.**

Glucocorticoids (GCs) are important anti-inflammatory and immunosuppressive agents that are the most widely prescribed drugs for the treatment of a broad spectrum of inflammatory and autoimmune disease entities. Unfortunately, GCs induce severe metabolic side effects, which complicate their use. One of the most significant side effects for patients treated with GCs is weight gain, specifically central fat accumulation, leading to a characteristic "buffalo hump" and obesity (1,2). Whereas white adipose tissue (WAT) stores excess energy, brown adipose tissue (BAT) has an opposite physiological function where it allows energy dissipation (3,4). An increasing amount of evidence indicates that the ability of mammals to resist body fat accumulation is linked to their ability to expand the number and activity of brown adipocytes within white fat depots (5–7). The activity of brown adipocytes within WAT is also correlated with blood glucose levels, insulin sensitivity, and body composition (8). Studies of alternative strategies to increase energy expenditure offer a new perspective on the conversion between brown and white adipocytes as a means of remodeling to increase energy disposal (5,9,10). Therefore, "browning" of white fat has

[1]Department of Geratology, The First Hospital Affiliated to Nanjing Medical University, Nanjing, People's Republic of China
[2]Department of General Surgery, The First Hospital Affiliated to Nanjing Medical University, Nanjing, People's Republic of China
[3]Metabolic Syndrome Research Center of Central South University, Institute of Metabolism and Endocrinology, The Second Xiangya Hospital of Central South University, Changsha, People's Republic of China
[4]Bone Research Program, ANZAC Research Institute, University of Sydney, Sydney, Australia

Corresponding authors: Guoxian Ding, dinggx@njmu.edu.cn, and Juan Liu, lioujane@njmu.edu.cn.

Received 11 March 2014 and accepted 15 August 2014.

This article contains Supplementary Data online at http://diabetes.diabetesjournals.org/lookup/suppl/doi:10.2337/db14-0395/-/DC1.

X.K. and J.Y. contributed equally to this work.

become a current focus in the ongoing fight against obesity.

GCs are powerful regulators of white adipocyte differentiation and have been reported to play an additional role in brown adipose function. Soumano et al. (11) reported that in a brown adipose cell line, GCs inhibit the transcriptional response of the uncoupling protein-1 (Ucp1) gene, a specific mitochondrial protein involved in the regulation of thermogenesis and energy expenditure in BAT. Strack et al. (12) also found that corticosterone decreases nonshivering thermogenesis and increases lipid storage in BAT of rats. Moreover, dexamethasone (DEX) was recently observed to decrease the expression of BAT-specific genes, including Ucp1, Cidea, Cox7a1, and Cox8b, and inhibits BAT thermogenesis in mice (13,14). However, the role of GCs in the browning of WAT remains largely undetermined. Given the action of GCs on the suppression of energy expenditure in BAT, the critical questions of the current study were whether GCs inhibit the functional "brown-like" adipocyte properties, and if so, what is the underlying mechanism?

microRNAs (miRNAs) are endogenously expressed, noncoding small RNAs (19–22 nucleotides) that regulate mRNA stability or protein translation through targeting the three prime untranslated regions (3′ UTRs) of mature mRNA (15,16). Increasing evidence indicates that GCs regulate multiple miRNAs in T cells (17,18). Thus, we hypothesized that GC regulation of miRNAs might play a role in the browning of WAT.

We examined the expression of >20 miRNAs that are regulated by GCs in human adipocytes. We identified that microRNA-27b (miR-27b) is upregulated in response to GC treatment and is a central upstream regulator of Prdm16 to control browning of WAT. Consequently, targeting miR-27b may promote energy expenditure mediated by WAT conversion to BAT and potentially prevent or attenuate GC-induced metabolic dysfunction.

## RESEARCH DESIGN AND METHODS

### Human Adipose Stromal Vascular Fraction Cell Culture and Microarray

Paired samples of abdominal subcutaneous and intra-abdominal omental adipose tissue were obtained from Chinese men ($n$ = 6) and women ($n$ = 6) who underwent open abdominal surgery (Supplementary Table 1). This was approved by the research ethics committee of Nanjing Medical University. All subjects gave written informed consent before taking part in the study. Human stromal vascular fraction (SVF) cells were isolated from subcutaneous adipose tissue (SAT) and visceral adipose tissue (VAT) samples as previously described (19) and cultured with 0.01 μmol/L DEX (control) or 1 μmol/L DEX (Supplementary Data).

### Animal Studies

C57BL/6J male mice (Model Animal Research Center of Nanjing University) were maintained on a 12-h light/dark cycle (Supplementary Data). All animal use protocols were reviewed and approved by the Animal Care Committee of the Model Animal Research Center of Nanjing University and were in accordance with Institutional Animal Care and Use Committee guidelines.

### In Vivo Gene Delivery: Tail Vein Injection With Lentiviruses

Lentiviruses encoding the antisense to miR-27b (antimiR-27b) with sequence of GCAGAACTTAGCCACTGTGAA or a scrambled control (scr-miR) were obtained from GeneChem Inc. (Shanghai, China). For in vivo gene delivery, mice were injected with $6 \times 10^7$ transducing units/mouse of each lentivirus in 100 μL PBS through tail veins after treatment with DEX for 6 weeks. Mice were killed on the 12th day after the lentiviral injection.

### Adipose Tissue Histology and Immunohistochemistry

The sections of SAT or VAT were incubated with anti-Ucp1 antibodies (Abcam) for 30 min at room temperature. The signals were detected using a biotinylated goat anti-rabbit secondary antibody (Vector Laboratories) in combination with the VECTASTAIN ABC Kit (Vector Laboratories) and DAB Substrate Kit (Vector Laboratories).

### Mouse Adipose SVF Cell Culture and Transfection

The SVF cells were isolated from inguinal and epididymal adipose tissue of 3-week-old male C57BL/6J mice (Supplementary Data).

### Chromatin Immunoprecipitation Assay

Chromatin in control and treated cells was cross-linked with 1% formaldehyde. Cells were incubated in lysis buffer (150 mmol/L NaCl, 25 mmol/L Tris [pH 7.5], 1% Triton X-100, 0.1% SDS, 0.5% deoxycholate) supplemented with protease inhibitor tablets and phenylmethylsulfonyl fluoride. DNA was fragmented (~500 base pairs) using a Branson 250 sonicator. Aliquots of lysates containing 200 μg protein were used for each immunoprecipitation reaction with anti-GC receptor (Santa Cruz) antibody or preimmune IgG. Precipitated genomic DNA was amplified by real-time PCR. Serial dilutions of genomic DNA extracted from normal cells were included with chromatin immunoprecipitation (ChIP) samples as standards to determine the amount of DNA being precipitated by a particular antibody.

### Luciferase Assay and Site-Directed Mutagenesis

Luciferase activities were assayed after transfection for 24 h using a luciferase reporter assay system (Promega). Experiments were routinely performed in triplicate wells and repeated three times.

### Measurement of Oxygen Consumption

Primary SVF cells were cultured in 24-well plates and differentiated as indicated (Seahorse Bioscience). Oxygen consumption rates (OCRs) were measured at basal glucose levels as well as with drugs disrupting the respiratory chain, including oligomycin (ATP synthase inhibitor, 1 μmol/L) (Sigma-Aldrich) and carbonyl cyanide p-trifluoromethoxyphenylhydrazone (FCCP) (uncoupler,

1 μmol/L) (Sigma-Aldrich). Finally, the mitochondrial respiration was blocked by 1 μmol/L rotenone (Sigma-Aldrich). The residual OCR was considered nonmitochondrial respiration.

### Statistics

Results are presented as mean ± SEM. Statistically significant differences were calculated using the Student *t* test. $P < 0.05$ was considered significant.

## RESULTS

### GCs Induce Glucose Intolerance and Fat Accumulation

Mice received DEX or placebo treatment for 6 weeks by daily injections. All mice treated with DEX gained significant body weight (Fig. 1*A*), developed glucose intolerance (Fig. 1*B*), and had site-specific increases in fat mass, such as SAT and VAT, compared with the placebo-treated group (Fig. 1*C* and *D*). The adipose tissues were further characterized by measuring adipocyte number (cells/field of view) in hematoxylin-eosin (H&E)–stained sections of SAT and VAT fat pads excised from mice following 6 weeks of DEX or placebo treatment. We observed that the adipocytes in SAT and VAT of DEX-treated mice appeared larger (Fig. 1*E*), and the cell number was significantly reduced compared with the placebo-treated mice (Fig. 1*F*). In addition, many browning cells were evident by the presence of many multilocular lipid droplets in SAT of placebo-treated mice. However, these browning cells were absent in SAT of DEX-treated mice (Fig. 1*E*).

### GCs Inhibit the Browning of WAT

DEX treatment significantly suppressed Ucp1 mRNA in both white adipose depots, with more potent inhibitory effects on SAT (80% decrease) than on VAT (50% decrease) compared with placebo treatment (Fig. 2*A*). In addition, a distinct type of Ucp1-positive multilocular adipocyte was observed in SAT of placebo-treated mice but not seen in DEX-treated mice (Fig. 2*B*), suggesting the role of GCs in the browning of WAT. Because DEX-treated mice developed glucose intolerance, this GC-induced fuel metabolism disorder could contribute to the altered WAT browning observed in GC-treated mice or vice versa. The SVF cells were isolated from SAT or VAT and differentiated with 1 μmol/L DEX concurrently during the first 4 days of cultures. The Ucp1 mRNA expression increased during adipocyte differentiation, peaking at day 4 (eight-fold higher than day 0) and then declining to the base levels in the SAT-derived cultures (Fig. 2*C*). In contrast, the Ucp1 mRNA expression was detectable at the same level seen in SAT cultures, but this level remained unchanged during differentiation in the VAT-derived cultures (Fig. 2*C*). To investigate the regulation and role of GCs in Ucp1 mRNA expression, we differentiated the SVF cells for 4 days in the absence or presence of DEX at a dose range of 0.1–10 μmol/L. DEX suppressed Ucp1 mRNA expression in a dose-dependent manner in both SAT- and VAT-derived cultures (Fig. 2*D*).

Continuous measurements of OCR were collected over 12 measurements (Fig. 2*E* and *F*). Consistent with

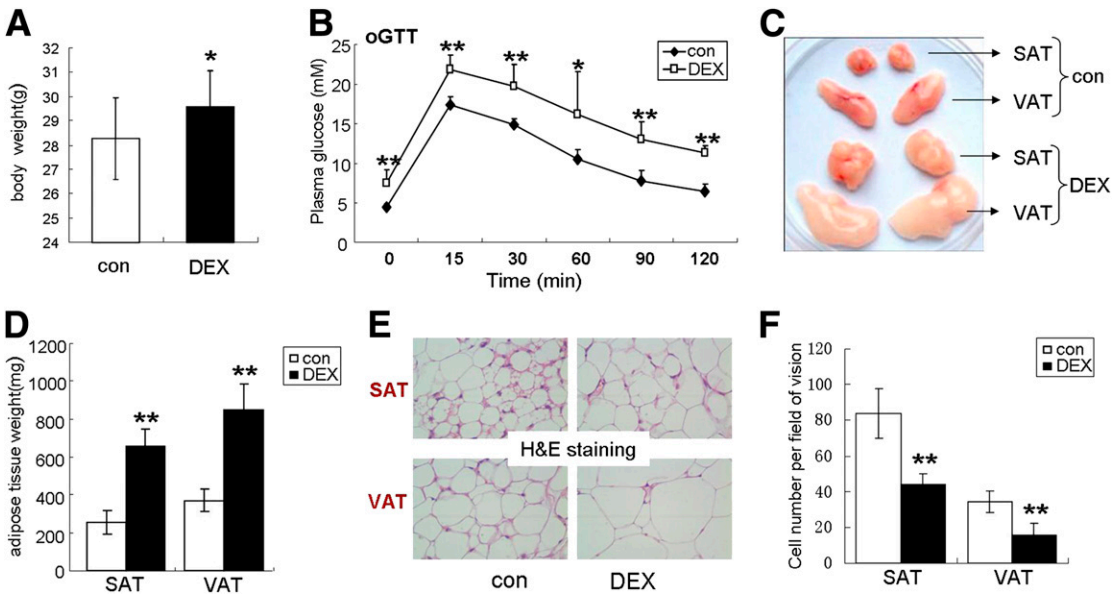


**Figure 1**—GCs induce glucose intolerance and fat accumulation. *A*: End point body weight of 12-week-old male mice treated with 5 mg/kg/day DEX or placebo (con) for 6 weeks. Data are mean ± SEM ($n = 12$). *$P < 0.05$. *B*: Oral glucose tolerance test (oGTT) in mice treated with either placebo or DEX for 6 weeks. Data are mean ± SEM ($n = 6$). *$P < 0.05$; **$P < 0.01$, DEX-treated group vs. control group. *C*: Representative images of SAT (subcutaneous adipocytes) and VAT (visceral adipocytes) fat pads isolated at the end point of treatment. *D*: SAT and VAT mass were measured by weight. Data are mean ± SEM ($n = 12$). **$P < 0.01$. *E*: Representative images of H&E-stained sections of SAT and VAT fat pads following 6 weeks of treatment. Original magnification ×200. *F*: Adipose cells per field of view were counted in H&E-stained sections of SAT and VAT fat pads. Data are mean ± SEM ($n = 5$). **$P < 0.01$.

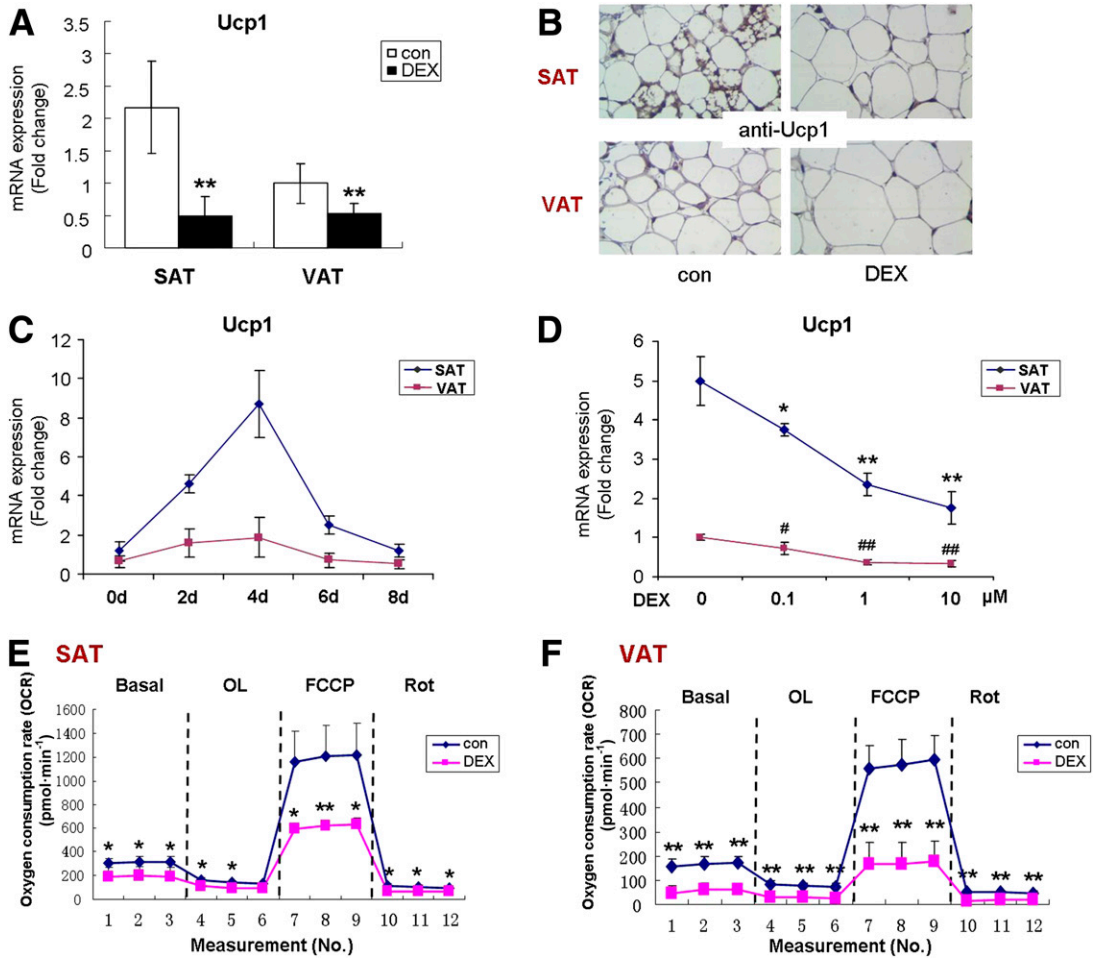


**Figure 2—**DEX inhibits the browning of white fat. *A*: Quantitative real-time PCR analysis of Ucp1 mRNA expression of SAT (subcutaneous adipose depots) and VAT (visceral adipose depots) in mice treated for 6 weeks with either placebo (con) or DEX. Data are mean ± SEM ($n$ = 10–12). $^{**}P < 0.01$, DEX-treated group vs. control group. *B*: Immunohistochemistry-stained Ucp1 sections of SAT and VAT fat pads following 6 weeks of treatment. Original magnification ×200. *C*: Quantitative real-time PCR analysis of Ucp1 mRNA expression during primary adipocyte differentiation. The SVF cells were isolated from SAT or VAT and differentiated for the time indicated under standard adipogenic conditions, including 1 μmol/L DEX complement in the first 4 days of culture. Experiments were repeated three times. Data are mean ± SEM ($n$ = 5). *D*: Primary SVF cells derived from SAT and VAT were differentiated for 4 days in the absence or presence of DEX at the dose range indicated. Ucp1 mRNA was analyzed by quantitative real-time PCR. Experiments were repeated three times. Data are mean ± SEM ($n$ = 4). $^{*}P < 0.05$; $^{**}P < 0.01$, DEX-treated SAT vs. its control; $\#P < 0.05$; $\#\#P < 0.01$, DEX-treated VAT vs. its control. *E* and *F*: OCRs were quantified at the basal condition as well as with drugs disrupting the respiratory chain (oligomycin [OL] [ATP synthase inhibitor, 1 μmol/L], FCCP [uncoupler, 1 μmol/L], and rotenone [Rot] [mitochondrial respiration block, 1 μmol/L]) by a Seahorse Bioscience XF24 analyzer in the primary SVF cells derived from SAT (*E*) or VAT (*F*) differentiated for 4 days with vehicle (con) or 1 μmol/L DEX treatment. Data are mean ± SEM ($n$ = 5). $^{*}P < 0.05$, $^{**}P < 0.01$.

the reduced Ucp1 gene expression, differentiation in the presence of 1 μmol/L DEX led to a marked decrease in the basal OCR. Furthermore, after the addition of an ATP synthase inhibitor (oligomycin) or a chemical uncoupler (FCCP), the OCR in DEX-treated adipocytes remained at significantly lower levels than the control in the SAT-derived cultures (Fig. 2*E*). Of note, although we did not observe an induction of Ucp1 in VAT adipocyte cultures (Fig. 2*C*), oxygen consumption was still detectable but at lower rates than observed in SAT cultures (Fig. 2*E*). DEX almost completely inhibited oxygen consumption in the VAT adipocyte cultures.

### GCs Upregulate miR-27b in Human Adipocytes

We next examined whether GCs have the same effect on Ucp1 expression in human primary adipocytes. We cultured primary SVF cells derived from human SAT and VAT under standard human adipogenic conditions with 0.01 μmol/L DEX (control) or 1 μmol/L DEX for 4 days. Similar to the results of mouse adipocyte cultures, the expression of Ucp1 mRNA levels in SAT-derived SVF cells were higher (more than fivefold) than that in VAT-derived SVF cells. The concentration of 1 μmol/L DEX significantly inhibited the expression of Ucp1 in both human SAT- and VAT-derived cultures (Fig. 3*A*).

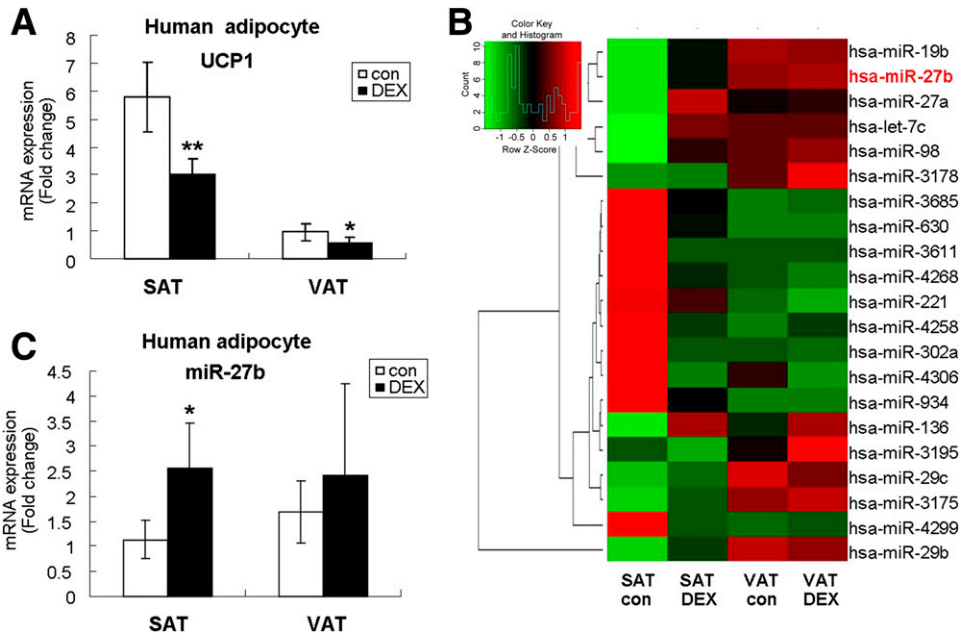


**Figure 3**—DEX upregulates miR-27b in human adipocytes. *A*: Human SVF cells isolated from SAT or VAT were cultured in a standard differentiation medium containing 0.01 μmol/L DEX (con) or 1 μmol/L DEX for 24 h. The expression of Ucp1 mRNA was determined by quantitative real-time PCR. Data are mean ± SEM ($n$ = 6). *$P$ < 0.05; **$P$ < 0.01, DEX vs. control. *B*: Heat map of miRNA array results from the samples treated with 0.01 μmol/L DEX (con) or 1 μmol/L DEX for 24 h. Red bars indicate higher expression, and green bars indicate lower expression. Black bars indicate the median expression between red and green bars. miR-27b is shown in red. *C*: Expression levels of miR-27b were validated by quantitative real-time PCR. Data are mean ± SEM ($n$ = 6). *$P$ < 0.05, DEX vs. control.

We performed miRNA microarray analysis. Array-based human miRNA expression profiles were determined in the primary adipocyte cultures derived from human SAT and VAT, as described previously, with incubation of 0.01 μmol/L DEX (control) or 1 μmol/L DEX for 24 h. Two distinct expression clusters of miRNAs were obtained by hierarchical clustering analysis (Fig. 3*B*). Of the 1,891 known and predicted human miRNAs, 11 were upregulated and 10 downregulated more than twofold in the primary adipocytes treated with DEX compared with control. As shown in Fig. 3*B*, the heat map highlights that among these miRNAs, miR-27b is most upregulated by 1 μmol/L DEX treatment in SVF cells derived from SAT. We further validated the expression of miR-27b in human SVF cell cultures by real-time PCR. As shown in Fig. 3*C*, the expression of miR-27b in the SVF cells derived from SAT was significantly upregulated by 1 μmol/L DEX after 24-h treatment, whereas expression of miR-27b in VAT-derived SVF cells showed no change following DEX treatment.

### GCs Transcriptionally Upregulate miR-27b in Mouse Adipocytes

Because human miR-27b sequences have 100% homology with mouse miR-27b (Supplementary Fig. 1), we validated the miR-27b expression in response to DEX treatment in murine adipocytes. We differentiated the murine SVF cells derived from SAT or VAT for 4 days in the absence or presence of DEX at a dose range of 0.1–10 μmol/L. Without DEX, miR-27b expression was 2.5-fold higher in VAT-derived adipocytes than in SAT-derived adipocytes (Fig. 4*A*). DEX upregulated miR-27b expression in SAT-derived adipocytes in a dose-dependent manner (Fig. 4*A*).

GC action is mediated by the GC receptor (GR), a ligand-inducible nuclear transcription factor (20,21). Binding to a consensus GR response element (GRE) is one of the mechanisms by which the ligand-activated GR regulates gene transcription (22). By sequence analysis, we identified a putative GRE site that is highly homologous to the consensus sequence of the GREs (Fig. 4*B*) at position −140 to −126 in the miR-27b promoter region. To determine whether GCs transcriptionally regulate miR-27b expression through GRE, we performed ChIP assays. Binding of GR to the GRE region in the miR-27b promoter was detected by ChIP assay, and DEX treatment led to a sevenfold enhanced binding of GR to the miR-27b promoter compared with base levels, whereas RU486, a potent antagonist of GR, completely blocked this DEX action (Fig. 4*C*). These results suggest that GCs transcriptionally regulate the miR-27b expression through a GR-mediated direct DNA-binding mechanism.

### miR-27b Negatively Regulates the Browning of WAT

As shown in Fig. 5*A*, miR-27b expression is lower in primary adipocytes derived from SAT than from VAT. Of note, there is an inverse relationship between the mRNA expression of Ucp1 and miR-27b (Fig. 5*A* and *B*). Furthermore, this negative correlation between miR-27b

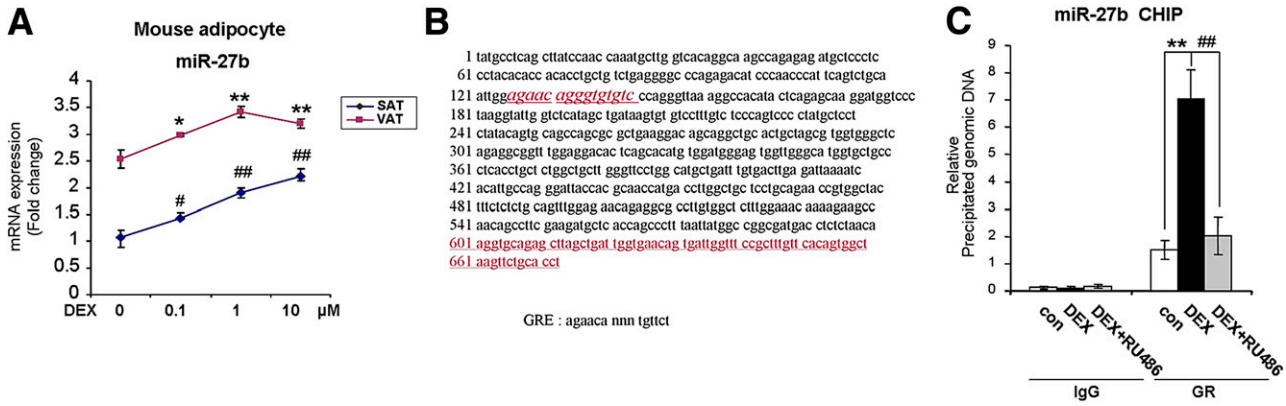


**Figure 4**—GCs transcriptionally upregulate miR-27b in mouse adipocytes. *A*: Quantitative real-time PCR analysis of miR-27b expression in primary adipocyte cultures in which SVF cells derived from mouse SAT or VAT were differentiated for 4 days in the absence or presence of DEX at the dose range indicated. Experiments were repeated three times. Data are mean ± SEM ($n$ = 4). *$P$ < 0.05; **$P$ < 0.01, DEX-treated SAT vs. its control (0); #$P$ < 0.05; ##$P$ < 0.01, DEX-treated VAT vs. its control (0). *B*: The promoter region at position −140 to −126 of miR-27b had high homology to the GRE consensus sequence. *C*: Quantitative real-time PCR of miR-27b promoter enriched by ChIP assays in SVF cells derived from mouse SAT or VAT treated with 1 μmol/L DEX and/or 10 μmol/L RU486 for 24 h as indicated under the differentiation conditions. Experiments were performed in triplicate. Data are mean ± SEM ($n$ = 4). **$P$ < 0.01, con vs. DEX; ##$P$ < 0.01, DEX vs. DEX + RU486 cells.

and Ucp1 expression can be seen over an 8-day time course (Figs. 2*C* and 5*C*). These data suggest that miR-27b may negatively regulate Ucp1 expression. To further investigate the role of miR-27b in the browning of WAT, we overexpressed miR-27b in SVF cells derived from SAT (Fig. 5*D*). Overexpression of miR-27b resulted in significant inhibition of the expression for the genes representative of brown adipocytes, including Ucp1, Cidea, Cox8b, Cox7a1, and Prdm16 (Fig. 5*E*) compared with the cells transfected with or without the scrambled oligonucleotide control (mimic-con). In addition, Western blot analysis indicated that Prdm16 and Ucp1 protein levels were also decreased (Fig. 5*F*). Of note, the mRNA expression of aP2, a marker of white mature adipocytes, was not altered by mimic-miR-27b transfection (Fig. 5*E*). Consistent with the inhibited expression of genes for browning, the oxygen consumption in mimic-miR-27b–transfected cells cultured under the same conditions as described for Fig. 5*E* was also markedly inhibited to the same levels as DEX treatment as assessed using a Seahorse Bioscience XF24 respirometry analyzer (Fig. 5*G*).

To determine whether the DEX suppression of the browning of WAT is through its induction of miR-27b expression, we antagonized miR-27b function by transfecting the SVF cells derived from SAT with antimiR-27b. The cells transfected with either antimiR-27b or scrambled miR-27b oligonucleotide control (scr-miR) were differentiated for 4 days in the presence or absence of 1 μmol/L DEX. As shown in Fig. 5*H*, antimiR-27b transfection efficiently blocked both constitutive and DEX-induced miR-27b expression. Antagonization of miR-27b function significantly increased the expression of Ucp1, Cidea, Cox8b, Cox7a1, and Prdm16 compared with scramble-control cells. In addition, antimiR-27b completely blocked the suppressive action of DEX on mRNA expression of these genes and restored expression levels to those seen in the scramble-control cells (Fig. 5*I*). Again, aP2 mRNA levels were not altered either by DEX or by antimiR-27b (Fig. 5*I*). Western blot analysis also indicated that Prdm16 and Ucp1 protein levels were increased in antimiR-27b transfected cells (Fig. 5*J*). Furthermore, although DEX inhibits oxygen consumption in the primary adipocytes, antimiR-27b completely negated the inhibitory effects of DEX on oxygen consumption (Fig. 5*K*).

### miR-27b Directly Targets Prdm16

By the miRNA target prediction analysis (www.targetscan.org), we identified a putative miR-27b target site at a highly conserved octamer seed motif within the 3′ UTR of Prdm16 (Supplementary Fig. 2). We cloned the 3′ UTR segment of Prdm16 containing the putative miR-27b target site (mPrdm16_3′ UTR-NM_022113; 3824–3831), or a mutated binding site for miR-27b on the Prdm16 3′ UTR, into a pMiRGLO luciferase reporter construct. The reporter constructs were cotransfected with mimic-miR-27b into HEK293T cells to determine the effects of miR-27b on luciferase translation. Luciferase reporter assays revealed that mimic-miR-27b reduced the activity of the reporter construct harboring a wild-type 3′ UTR but not the mutated 3′ UTR (Fig. 6*A*). Together with the Western blot analysis in Fig. 5*J* showing an increase in Prdm16 protein levels in antimiR-27b transfected cells, these data demonstrate that miR-27b specifically targets the 3′ UTR of the Prdm16 translation. To further investigate whether PRDM16 directly mediates the inhibition of the browning effect exerted by miR-27b, we knocked down PRDM16 mRNA in antimiR-27b–transfected primary adipocytes through a lentiviral-based expression system driving the production of PRDM16 short hairpin RNA (shRNA) (Supplementary Fig. 3). Compared

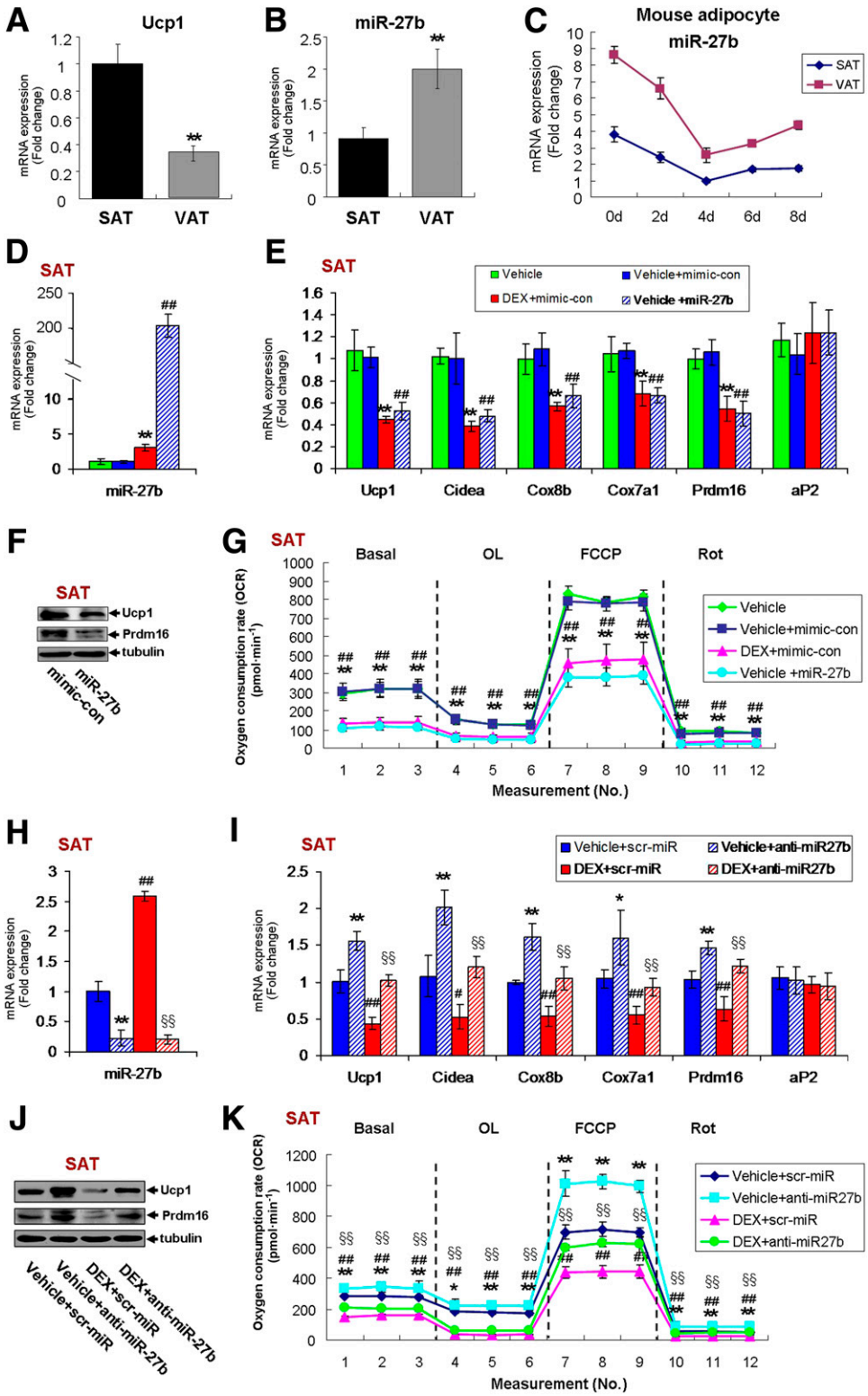


**Figure 5**—miR-27b is a potent negative regulator of the browning effect on white adipocytes. *A* and *B*: Quantitative real-time PCR analysis of Ucp1 and miR-27b expression in primary adipocyte cultures of SVF cells isolated from mouse SAT and VAT following differentiation for 4 days in the absence of DEX. Data are mean ± SEM ($n$ = 4). $^{**}P < 0.01$. *C*: Quantitative real-time PCR analysis of miR-27b expression during primary adipocyte differentiation. The SVF cells were isolated from SAT or VAT and differentiated for the time indicated under adipogenic conditions with 1 μmol/L DEX complement. Data are mean ± SEM ($n$ = 5). *D*: miR-27b mRNA expression in SVF cells from SAT by standard differentiation (control) or transfecting with either mimic-con (vehicle + mimic-con) or mimic-miR-27b (vehicle + miR-27b) 4 days after differentiation. A concentration of 1 μmol/L DEX (DEX + mimic-con) presents as positive control. Data are mean ± SEM ($n$ = 4). $^{**}P < 0.01$, vehicle + mimic-con vs. DEX + mimic-con; $^{\#\#}P < 0.01$, vehicle + mimic-con vs. vehicle + miR-27b. *E*: Overexpression of miR-27b significantly reduced mRNA levels of BAT signature genes to the same level of DEX-treated control adipocytes. Data are mean ± SEM

with control cells, antimiR-27b knockdown efficacy was 90% for miR-27b mRNA in antimiR-27b and in the double-knockdown (antimiR-27b + short half-life green fluorescent protein [shGFP] and antimiR-27b + PRDM16 shRNA) cells derived from SAT (Fig. 6*B*). Consequently, knockdown of Prdm16 blocked antimiR-27b induction of Prdm16 downstream target genes, including Ucp1, Cidea, Cox8b, and Cox7a1, compared with the anticontrol cells (Fig. 6*C*). The loss of Prdm16 expression also blocked the miR-27b actions on cell oxygen consumption (Fig. 6*D*).

### AntimiR-27b Treatment Protects From GC-Induced Obesity and Insulin Resistance and Enhances Oxygen Consumption In Vivo

We used a lentiviral system to deliver antimiR-27b in vivo. Compared with DEX-treated scramble-control mice, antimiR-27b blocking efficacy was 75% for miR-27b mRNA in SAT and 50% in VAT of mice treated with DEX and antimiR-27b virus (Fig. 7*A*). On day 12 after lentivirus injection, we performed indirect calorimetry. Oxygen consumption (Fig. 7*B* and *C*) and carbon dioxide production (Fig. 7*D*) were significantly enhanced during both light and dark phases for the antimiR-27b–treated mice. The heat production (Fig. 7*E*) of antimiR-27b mice was also higher than in scr-miR–treated control mice. Because no differences in the food intake (Fig. 7*F*) and physical activity (Fig. 7*G*) were found between the two DEX-treated groups, we next analyzed the impact of miR-27b on glucose metabolism. As expected, after insulin administration, DEX-treated mice became insulin resistant. In contrast, the DEX + antimiR-27b–treated mice exhibited the same response over the course of the experiment as the placebo-treated mice (Fig. 7*H*), implying that inhibition of miR-27b improved DEX-induced insulin resistance. At the end point of treatment, mice in the DEX-treated group gained significantly in body weight compared with placebo-treated mice, whereas the mice receiving both DEX and antimiR-27b treatments remained the same weight as the placebo-treated mice (Fig. 7*I*). Similarly, SAT fat mass and VAT fat mass was significantly increased in DEX-treated mice compared with placebo-treated mice, whereas they were similar in placebo-treated and DEX + antimiR-27b–treated animals (Fig. 7*J* and *K*). Moreover, in the placebo-treated and DEX + antimiR-27b–treated mice, histological analysis of the H&E-stained sections of SAT and VAT revealed that the adipocytes in these tissues were smaller (Fig. 7*L*) and had a markedly increased cell number per field of view than that seen in DEX-treated mice (Fig. 7*M*). We observed that Ucp1-positive cells were also readily detected in the WAT of the placebo-treated and DEX + antimiR-27b–treated mice, but few were detected in the DEX-treated mice (Fig. 7*N*). In addition, a significant increase in the mRNA expression of Ucp1 in WAT (both SAT and VAT) was observed in DEX + antimiR-27b–treated mice compare with DEX-treated mice, although antimiR-27b treatment did not fully correct the DEX-suppressed Ucp-1 expression to the levels seen in the placebo group (Fig. 7*O*). Taken together, these findings suggest that the antimiR-27b–induced browning effect in WAT is metabolically functional and has a favorable impact on glucose metabolism in mice.

## DISCUSSION

Long-term GC treatment induces severe metabolic side effects, including weight gain, insulin resistance, and diabetes. These unwanted outcomes frequently limited their use and clinical benefits. However, the precise cellular and molecular pathways by which GCs affect fuel metabolism are still largely obscure. The current study demonstrates that miR-27b plays a central role in the pathogenesis of the detrimental effects of high-dose GCs on fat and energy metabolism (Fig. 8). This finding could provide a potential target in the prevention of GC-induced obesity and metabolic dysfunction (23–25).

We recently showed that the expression of BAT-specific genes, including Ucp1, Cidea, Cox7a1, and Cox8b, is significantly decreased in the BAT of DEX-treated mice (13). We now demonstrate that GCs also inhibit browning of WAT and the thermogenic program in WAT, which lead to central fat accumulation. Under physiologic conditions (without cold exposure), the brown-like adipocytes can be detected in SAT in vivo. Consistent with the in vivo data, adipocyte precursors

($n$ = 4). $^{**}P < 0.01$, vehicle + mimic-con vs. DEX + mimic-con; $^{\#\#}P < 0.01$, vehicle + mimic-con vs. vehicle + miR-27b. *F*: Western blot of whole-cell lysates from 4-day differentiated SVF cells following transfection with mimic-miR-control (mimic-con) and mimic-miR-27b (miR-27b). *G*: OCRs were quantified at basal conditions as well as with drugs disrupting the respiratory chain (oligomycin [OL], FCCP [uncoupler], and rotenone [Rot]) of the cells under the same conditions as *D*. Data are mean ± SEM ($n$ = 5). $^{**}P < 0.01$, vehicle + mimic-con vs. DEX + mimic-con; $^{\#\#}P < 0.01$, vehicle + mimic-con vs. vehicle + miR-27b. *H*: Compared with scrambled-control (scr-miR) cells, antimiR-27b blocking efficacy was 90% for miR-27b mRNA in SVF cells from SAT by transfecting with antimiR-27b following 4-day differentiation. Data are mean ± SEM ($n$ = 4). $^{**}P < 0.01$, vehicle + scr-miR vs. vehicle + antimiR-27b; $^{\#\#}P < 0.01$, DEX + scr-miR vs. DEX + antimiR-27b; §§$P <$ 0.01 DEX + scr-miR vs. DEX + antimiR-27b cells. *I*: Quantitative real-time PCR analysis of expression of BAT signature genes compared with scrambled cells (vehicle + scr-miR), antimiR-27b cells (vehicle + antimiR-27b), 1 μmol/L DEX-treated anticontrol cells (DEX + scr-miR), and antimiR-27b cells (DEX + antimiR-27b) for 4 days under differentiation culture conditions. Data are mean ± SEM ($n$ = 4). $^{*}P < 0.05$; $^{**}P < 0.01$, vehicle + scr-miR vs. vehicle + antimiR-27b; $^{\#}P < 0.05$; $^{\#\#}P < 0.01$, vehicle + scr-miR vs. DEX + scr-miR; §§$P <$ 0.01 DEX + scr-miR vs. DEX + antimiR-27b cells. *J*: Western blot of whole-cell lysates from 4-day differentiated SVF cells treated the same as in *H*. *K*: OCRs were quantified in the cells described in *H*. Data are mean ± SEM ($n$ = 5). $^{**}P < 0.01$, vehicle + scr-miR vs. vehicle + antimiR-27b; $^{\#\#}P <$ 0.01 vehicle + scr-miR vs. DEX + scr-miR; §§$P <$ 0.01 DEX + scr-miR vs. DEX + antimiR-27b cells.

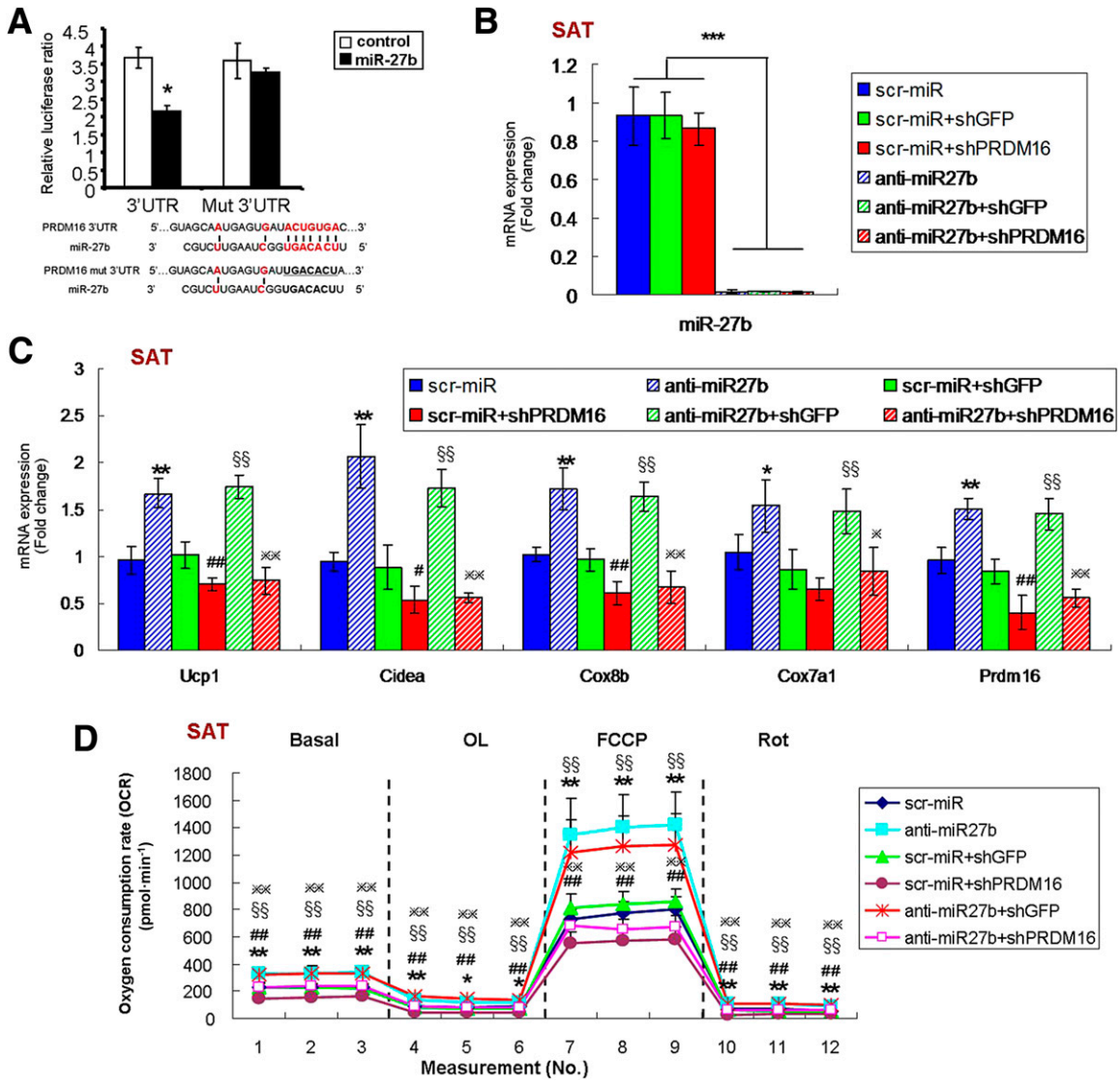


**Figure 6**—miR-27b directly targets Prdm16. *A*: The 3′ UTR of the Prdm16 gene contains the predicted binding site for miR-27b as shown by red sequences and is cloned into pMiRGLO vector (Prdm16 3′ UTR). In the mutant construct (Prdm16 Mut3′ UTR), the corresponding binding sequences were mutated as indicated in black. Luciferase reporter assay was used to examine the interactions between miR-27b and the predicted target site in the Prdm16 3′ UTR. Plasmids with the Prdm16 3′ UTR or a mutated 3′ UTR were cotransfected with mimic-miR-27b (miR-27b) or mimic-miR-control (control) into HEK293 cells. Experiments were performed in triplicate wells and repeated three times. Data are mean ± SEM. $^{*}P < 0.05$. *B*: Compared with anticontrol (scr-miR, scr-miR + shGFP, scr-miR + shPrdm16) cells, antimiR-27b blocking efficacy was 90% for miR-27b mRNA (quantitative real-time PCR) in SVF cells from mouse SAT by transfecting with antimiR-27b (antimiR-27b, antimiR-27b + shGFP) or with both antimiR-27b and Prdm16 shRNA (antimiR-27b + shPrdm16) following 4-day differentiation in 1 μmol/L DEX complement. Data are mean ± SEM ($n = 4$). $^{***}P < 0.001$. *C*: Quantitative real-time PCR analyses were also conducted for Ucp1, Cidea, Cox8b, Cox7a1, and Prdm16 in SAT-derived cells under the same conditions as *B*. Experiments were repeated three times. Data are mean ± SEM ($n = 4$). $^{*}P < 0.05$; $^{**}P < 0.01$, scr-miR vs. antimiR-27b; $\#P < 0.05$; $\#\#P < 0.01$, scr-miR + shGFP vs. scr-miR + shPrdm16; §§$P < 0.01$, scr-miR + shGFP vs. antimiR-27b + shGFP; ※$P < 0.05$; ※※$P < 0.01$, antimiR-27b + shGFP vs. antimiR-27b + shPrdm16. *D*: OCRs were quantified in cell cultures under the same conditions as *B* and *C*. Data are mean ± SEM ($n = 5$). $^{*}P < 0.05$; $^{**}P < 0.01$, scr-miR vs. antimiR-27b; $\#\#P < 0.01$, scr-miR + shGFP vs. scr-miR + shPrdm16; §§$P < 0.01$, scr-miR + shGFP vs. antimiR-27b + shGFP; ※※$P < 0.01$, antimiR-27b + shGFP vs. antimiR-27b + shPrdm16. OL, oligomycin; Rot, rotenone.

isolated from the SAT of mice kept at room temperature can be more efficiently differentiated toward brown adipocytes than preadipocytes derived from VAT as determined by Ucp1 mRNA levels and oxygen consumption. DEX inhibited brown adipocyte differentiation and the thermogenic activity in SAT in a dose-dependent manner. Of note, these effects of DEX were also observed in VAT cultures, although brown adipocyte differentiation was not clearly detected. Similar results were seen in human adipocyte cultures. DEX inhibition of Ucp1 expression was inversely correlated with the expression of miR-27b.

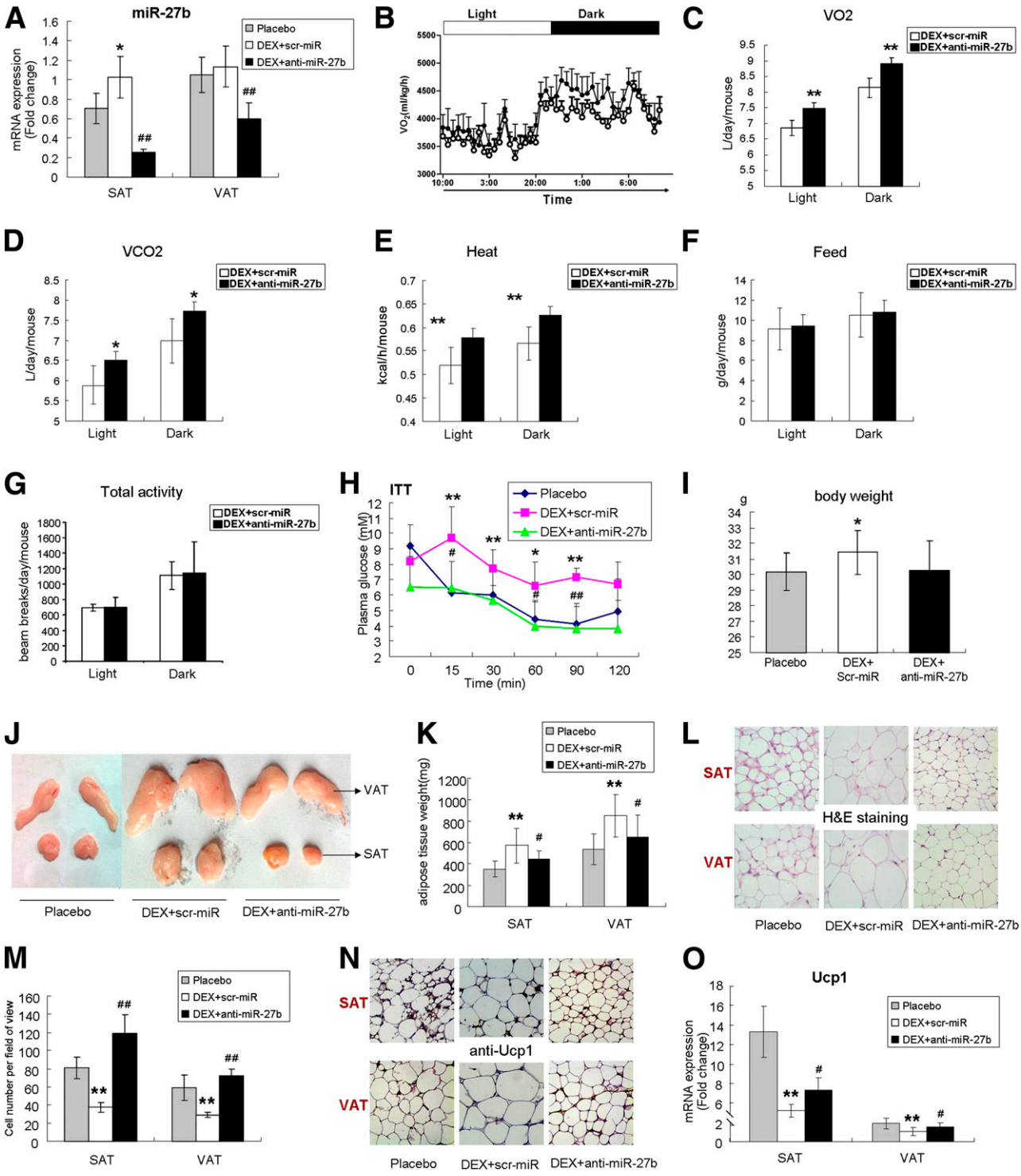


**Figure 7—**AntimiR-27b induces browning of WAT and increases nonshivering thermogenesis in vivo and rescues the GC-induced obesity. *A*: Compared with scrambled-control mice, antimiR-27b blocking efficacy was 75% for miR-27b mRNA in SAT and 50% in VAT from mice transfected with $6 \times 10^7$ transducing units/mouse of antimiR-27b (DEX + antimiR-27b) or scrambled-control (DEX + scr-miR) lentivirus through tail vein injection after 6 weeks of DEX treatment. The mice treated with placebo presented as negative control. Data are mean ± SEM ($n$ = 10–12). *$P$ < 0.05, placebo vs. DEX + scr-miR; ##$P$ < 0.01, DEX + scr-miR vs. DEX + antimiR-27b. *B*: On day 12 after lentivirus injection, real-time measurements of oxygen consumption were taken every 30 min in individually housed DEX + scr-miR and DEX + antimiR-27b mice. Data are mean ± SEM ($n$ = 6). *C–H*: Energy expenditure during a 24-h period is reported as $VO_2$ (*C*) and $VCO_2$ (*D*), and thermogenesis (heat) (*E*), food intake (*F*), and physical activity (*G*) were measured synchronously. Data are mean ± SEM ($n$ = 6). *$P$ < 0.05; **$P$ < 0.01, DEX + scr-miR vs. DEX + antimiR-27b. *H*: Insulin tolerance test (ITT). Blood glucose levels were measured after a 6-h fast (time 0) and at the indicated times after an intraperitoneal injection of insulin in placebo, DEX + scr-miR, and DEX + antimiR-27b mice. Data are mean ± SEM ($n$ = 6). *$P$ < 0.05; **$P$ < 0.01, placebo vs. DEX + scr-miR; #$P$ < 0.05; ##$P$ < 0.01, DEX + scr-miR vs. DEX + antimiR-27b. *I*: Body weight of mice on the day 12 following tail vein injection. Data are mean ± SEM ($n$ = 15). *$P$ < 0.05, placebo vs. DEX + scr-miR.

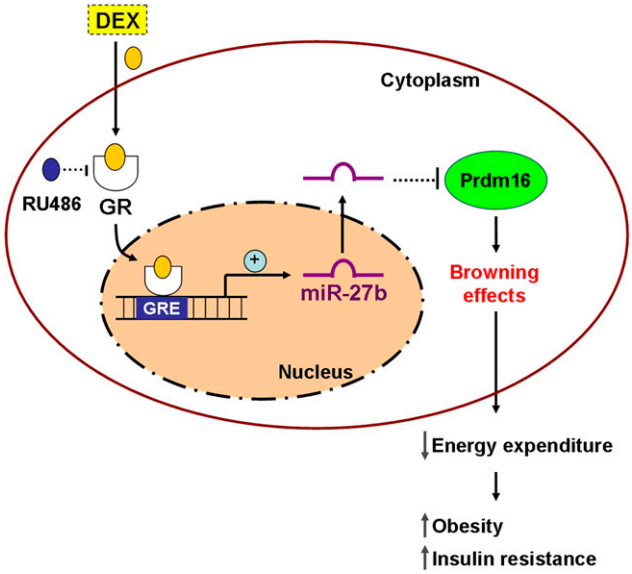


**Figure 8**—Schematic model of the action of GCs on browning effects of WAT in mice. Exogenous GCs transcriptionally upregulate the miR-27b expression. The GC-induced miR-27b then suppresses both Prdm16 mRNA and protein levels, which results in a downregulation of Ucp1. The decreased Ucp1 results in the low energy expenditure. The low energy expenditure consequently causes, or at least in part contributes to, the GC-induced fat accumulation and insulin resistance.

Several studies revealed that miR-27b is involved in the regulation of adipogenesis and the thermogenic program (26–28). The current study discovered that miR-27b is a GC target miRNA. Using ChIP assay, we demonstrated that this miRNA is transcriptionally induced by GC through GRE binding located in the miR-27b promoter region. miR-27b is constitutively expressed in primary adipocytes. The adipocyte cultures derived from VAT had 2–2.5 times more miR-27b than SAT cultures, and its expression was negatively correlated with the expression of Ucp1. Overexpression of miR-27b in the SAT precursors inhibited not only the expression of Ucp1, Cidea, Cox7a1, Cox8b, and Prdm16 but also the OCR at day 4 after differentiation induction, indicating that miR-27b inhibits brown adipose differentiation of WAT preadipocytes. Conversely, inhibition of miR-27b function in the SAT precursors using antimiR-27b completely blocked the inhibitory action of DEX on the expression of Ucp1, Cidea, Cox7a1, and Cox8b and the OCR at day 4 after differentiation induction with 1 μmol/L DEX concurrently, indicating that miR-27b mediates the adverse effects of DEX on fat accumulation through its inhibitory action on browning and energy expenditure.

To determine whether antagonizing GC-induced miR-27b functions can rescue or reverse GC-induced metabolic dysfunction, such as central fat accumulation and energy metabolism in vivo, we used a lentivirus system to deliver antimiR-27b. Although there was no difference in body weight between the DEX-treated mice receiving lentivirus containing antimiR-27b or scrambled control (scr-miR), the subcutaneous fat mass and visceral fat mass were significantly reduced in the antimiR-27b–treated mice compared with the scr-miR–treated mice. Although the food intake and total physical activity remained unchanged, the heat production, oxygen consumption, and carbon dioxide production were significantly enhanced in the antimiR-27b–treated mice. In addition, DEX-impaired glucose metabolism was improved in the antimiR-27b–treated mice compared with the scr-miR–treated mice. These results indicate that miR-27b may mediate GC-induced fat accumulation and fuel metabolism by inhibiting adipose tissue energy expenditure. This finding highlights the potential importance of the direct effects of miR-27b on adipose tissue.

Mounting evidence suggests that miRNAs play an essential role in posttranscriptional regulation of target genes (29,30). Furthermore, studies have suggested that miR-133 controls brown adipogenesis in skeletal muscle and BAT by targeting the 3′ UTR of Prdm16 (31,32). Therefore, we propose a role for miR-27b in the posttranscriptional regulation of Prdm16. We identified a putative miR-27b target site within the Prdm16 3′ UTR. Mutation of that site eliminated the capacity of miR-27b to downregulate the expression of luciferase reporters containing the Prdm16 3′ UTR. As expected, the mutant miR-27b expression vector did not affect the expression of the luciferase-Prdm16 3′ UTR constructs. To investigate whether the increase in brown adipose differentiation after miR-27b inhibition could be blocked by Prdm16 silencing, we simultaneously knocked down Prdm16 and miR-27b in DEX-treated preadipocytes derived from SAT. Knockdown of Prdm16 fully reversed the antimiR-27b–increased expression of Prdm16 downstream target genes, including Ucp1, Cidea, Cox7a1, and Cox8b, in SAT preadipocytes. These results indicate that the increase in Prdm16 by inhibition of GC-induced miR-27b is essential for the observed effects in vitro and in vivo.

*J*: Representative images of SAT and VAT fat pads isolated at the end point of treatment (12 days after lentivirus injection). *K*: SAT and VAT mass was measured by weight. Data are mean ± SEM ($n$ = 15). $^{**}P < 0.01$, placebo vs. DEX + scr-miR; $\#P < 0.05$, DEX + scr-miR vs. DEX + antimiR-27b. *L*: Representative images of H&E-stained sections of SAT and VAT fat pads. Original magnification ×200. *M*: Adipose cells per field of view were counted in H&E-stained sections of SAT and VAT fat pads. Data are mean ± SEM ($n$ = 5). $^{**}P < 0.01$, placebo vs. DEX + scr-miR; $\#\#P < 0.01$, DEX + scr-miR vs. DEX + antimiR-27b. *N*: Immunohistochemistry-stained Ucp1 sections of SAT and VAT fat pads. Original magnification ×200. *O*: Quantitative real-time PCR analysis of Ucp1 mRNA expression of SAT and VAT in mouse groups as indicated. Data are mean ± SEM ($n$ = 10–12). $^{**}P < 0.01$, placebo vs. DEX + scr-miR; $\#P < 0.05$, DEX + scr-miR vs. DEX + antimiR-27b.

In summary, the data show that miR-27b is activated by GCs and point to a critical role for miR-27b in the control of the browning of WAT through Prdm16. These findings suggest that miR-27b may represent a promising therapeutic target for preventing GC-induced obesity and metabolic syndrome.

**Funding.** This work was supported by grants from the National Natural Science Foundation of China (81170796 and 81370950), the Program for Development of Innovative Research Team in The First Affiliated Hospital of Nanjing Medical University (20113012), and grants from the National Natural Science Youth Foundation of China (30900504) to J.L. and the Priority Academic Program Development of Jiangsu Higher Education Institutions to G.D.

**Duality of Interest.** No potential conflicts of interest relevant to this article were reported.

**Author Contributions.** X.K., J.Y., J.B., and S.L. contributed to the in vitro experiments and data analyses. H.Q. and L.Wu. contributed to the lentiviral production and further transfection experiments. W.D., L.Wa., and J.Z. contributed to the in vivo experiments and data analyses. F.Z. contributed human materials. Y.L., F.H., and F.L. contributed to the oxygen consumption experiments. H.Z. and J.L. contributed to the project design, conduct of the experiments, and writing of the manuscript. G.D. contributed to the project concept, experimental design, data analysis, and writing of the manuscript. G.D. is the guarantor of this work and, as such, had full access to all the data in the study and takes responsibility for the integrity of the data and the accuracy of the data analysis.

## References

1. Veyrat-Durebex C, Deblon N, Caillon A, et al. Central glucocorticoid administration promotes weight gain and increased 11β-hydroxysteroid dehydrogenase type 1 expression in white adipose tissue. PLoS One 2012;7:e34002
2. Spencer SJ, Tilbrook A. The glucocorticoid contribution to obesity. Stress 2011;14:233–246
3. Frühbeck G, Becerril S, Sáinz N, Garrastachu P, García-Velloso MJ. BAT: a new target for human obesity? Trends Pharmacol Sci 2009;30:387–396
4. Stephens M, Ludgate M, Rees DA. Brown fat and obesity: the next big thing? Clin Endocrinol (Oxf) 2011;74:661–670
5. Boström P, Wu J, Jedrychowski MP, et al. A PGC1-α-dependent myokine that drives brown-fat-like development of white fat and thermogenesis. Nature 2012;481:463–468
6. Wang L, Teng R, Di L, et al. PPARα and Sirt1 mediate erythropoietin action in increasing metabolic activity and browning of white adipocytes to protect against obesity and metabolic disorders. Diabetes 2013;62:4122–4131
7. Bartelt A, Heeren J. Adipose tissue browning and metabolic health. Nat Rev Endocrinol 2014;10:24–36
8. Wu J, Cohen P, Spiegelman BM. Adaptive thermogenesis in adipocytes: is beige the new brown? Genes Dev 2013;27:234–250
9. Qiang L, Wang L, Kon N, et al. Brown remodeling of white adipose tissue by SirT1-dependent deacetylation of Pparγ. Cell 2012;150:620–632
10. Seale P, Conroe HM, Estall J, et al. Prdm16 determines the thermogenic program of subcutaneous white adipose tissue in mice. J Clin Invest 2011;121:96–105
11. Soumano K, Desbiens S, Rabelo R, Bakopanos E, Camirand A, Silva JE. Glucocorticoids inhibit the transcriptional response of the uncoupling protein-1 gene to adrenergic stimulation in a brown adipose cell line. Mol Cell Endocrinol 2000;165:7–15
12. Strack AM, Bradbury MJ, Dallman MF. Corticosterone decreases nonshivering thermogenesis and increases lipid storage in brown adipose tissue. Am J Physiol 1995;268:R183–R191
13. Liu J, Kong X, Wang L, et al. Essential roles of 11β-HSD1 in regulating brown adipocyte function. J Mol Endocrinol 2013;50:103–113
14. Poggioli R, Ueta CB, Drigo RA, Castillo M, Fonseca TL, Bianco AC. Dexamethasone reduces energy expenditure and increases susceptibility to diet-induced obesity in mice. Obesity (Silver Spring) 2013;21:E415–E420
15. Wahid F, Shehzad A, Khan T, Kim YY. MicroRNAs: synthesis, mechanism, function, and recent clinical trials. Biochim Biophys Acta 2010;1803:1231–1243
16. Bartel DP. MicroRNAs: target recognition and regulatory functions. Cell 2009;136:215–233
17. Davis TE, Kis-Toth K, Szanto A, Tsokos GC. Glucocorticoids suppress T cell function by up-regulating microRNA-98. Arthritis Rheum 2013;65:1882–1890
18. Molitoris JK, McColl KS, Distelhorst CW. Glucocorticoid-mediated repression of the oncogenic microRNA cluster miR-17~92 contributes to the induction of Bim and initiation of apoptosis. Mol Endocrinol 2011;25:409–420
19. Bujalska IJ, Kumar S, Hewison M, Stewart PM. Differentiation of adipose stromal cells: the roles of glucocorticoids and 11beta-hydroxysteroid dehydrogenase. Endocrinology 1999;140:3188–3196
20. Kassel O, Herrlich P. Crosstalk between the glucocorticoid receptor and other transcription factors: molecular aspects. Mol Cell Endocrinol 2007;275:13–29
21. Schoneveld OJ, Gaemers IC, Lamers WH. Mechanisms of glucocorticoid signalling. Biochim Biophys Acta 2004;1680:114–128
22. Dostert A, Heinzel T. Negative glucocorticoid receptor response elements and their role in glucocorticoid action. Curr Pharm Des 2004;10:2807–2816
23. Reinehr T, Kulle A, Wolters B, et al. Relationships between 24-hour urinary free cortisol concentrations and metabolic syndrome in obese children. J Clin Endocrinol Metab 2014;99:2391–2399
24. Iwasaki Y, Takayasu S, Nishiyama M, et al. Is the metabolic syndrome an intracellular Cushing state? Effects of multiple humoral factors on the transcriptional activity of the hepatic glucocorticoid-activating enzyme (11beta-hydroxysteroid dehydrogenase type 1) gene. Mol Cell Endocrinol 2008;285:10–18
25. Stimson RH, Walker BR. Glucocorticoids and 11beta-hydroxysteroid dehydrogenase type 1 in obesity and the metabolic syndrome. Minerva Endocrinol 2007;32:141–159
26. Sun L, Trajkovski M. MiR-27 orchestrates the transcriptional regulation of brown adipogenesis. Metabolism 2014;63:272–282
27. Kang T, Lu W, Xu W, et al. MicroRNA-27 (miR-27) targets prohibitin and impairs adipocyte differentiation and mitochondrial function in human adipose-derived stem cells. J Biol Chem 2013;288:34394–34402
28. Allen DL, Loh AS. Posttranscriptional mechanisms involving microRNA-27a and b contribute to fast-specific and glucocorticoid-mediated myostatin expression in skeletal muscle. Am J Physiol Cell Physiol 2011;300:C124–C137
29. Filipowicz W, Bhattacharyya SN, Sonenberg N. Mechanisms of post-transcriptional regulation by microRNAs: are the answers in sight? Nat Rev Genet 2008;9:102–114
30. Siomi H, Siomi MC. Posttranscriptional regulation of microRNA biogenesis in animals. Mol Cell 2010;38:323–332
31. Yin H, Pasut A, Soleimani VD, et al. MicroRNA-133 controls brown adipose determination in skeletal muscle satellite cells by targeting Prdm16. Cell Metab 2013;17:210–224
32. Trajkovski M, Ahmed K, Esau CC, Stoffel M. MyomiR-133 regulates brown fat differentiation through Prdm16. Nat Cell Biol 2012;14:1330–1335